ADVANCED MATERIALS TECHNOLOGIES
www.advmattechnol.de

Selectively Stiffening Garments Enabled by Cellular Composites

*Junghan Kwon, Inrak Choi, Myungsun Park, Jeongin Moon, Bomin Jeong, Prabhat Pathak, Jooeun Ahn, and Yong-Lae Park**

Recent efforts on wearable robots have focused on augmenting the motor performance and/or protecting the wearer's body with lightweight structures. However, providing human-scale force and structural stiffness usually conflicts with the wearability. Inspired by sandwich-structured composites with high structural strengths, widely employed in both nature and man-made structures, a mechanism of selectively stiffening garments (SSGs) utilizing anisotropic cellular cores and rubber-laminated face sheets is proposed. While the proposed mechanism shows a high compliance allowing for conformity to the wearer's body when unjammed, it provides a significantly high force density when jammed, compared to conventional jamming methods, allowing for the ability to adjust mechanical properties based on the designs and materials. In this paper, various designs of the sandwich jamming structures for the SSGs with analytical characterizations and experimental validations are introduced. Potential applications for force and motion assistance are also demonstrated and impacted mitigation.

1. Introduction

What if a garment can harden itself depending on the task that the wearer undertakes? One of the long-term goals of functional garments is to improve the wearer's physical performances.[1] For example, compression sportswear reduces muscle strain by providing heat[2] and stabilizes the joints by stiffening the structure.[3] Orthoses assist specific body parts by limiting the ranges of motion.[4] Rigid protective gears, such as hip and chest guards, protect the wearer by distributing or absorbing impacts.[5] However, conventional functional garments always maintain their mechanical properties the same, since their performances heavily rely on the inherent material properties. Therefore, these permanent properties often cause discomfort and limit the wearer's activities in spite of the benefits in certain situations. Performance augmentation of a human body is also one of the long-standing challenges in robotics that researchers have tried to tackle with various technologies of wearable robots.[6] The main purpose of wearable robots is to provide additional forces for the wearer through active mechatronic systems for different motions, such as lifting,[7] grasping,[8] or walking.[9,10]

The concept of this article, the selective stiffening garment (SSG), draws upon the synergy between functional clothing and soft robotics[11] (**Figure 1**). We hypothesize that the wearer can benefit from the garment in two different aspects. First, it provides a physiological advantage in the musculoskeletal system (Figure 1a). The stiffening structure can selectively lock the kinematic chain of the body and support the weights of the body segments, reducing the level of muscle activation. Second, the garment can play a role of a protective layer. The hardened structure can form a hard outer shell that provides the wearer with additional protection and force, as shown in the "second skin" examples (Figure 1b).

The SSG can be realized by the mechanism of variable stiffness.[11] While several approaches have been proposed, including mechanical locking,[12] magnetorheological fluids,[13] electrostatic adhesion,[14] and thermally activated materials[15–17] one promising method is vacuum-based jamming of using particles,[18–24] fibers,[25–27] layers,[28–31] fabrics,[32,33] or even combinations of two or more of these methods.[34,35] The major advantages of fast transition between states, low cost, easy fabrication, and safe interaction with humans, make the jamming method attractive for various applications, including wearable devices,[36–39] grippers,[40] and manipulators.[41,42]

To be practical, the SSG should meet several requirements. First, the garment should be lightweight and comfortable so that it does not degrade the wearer's own physical ability. Second, when activated, the garment should be stiff enough to withstand the bending moment applied by external impacts as well as the wearer's body weight. Third, the garment should

J. Kwon
Harvard John A. Paulson School of Engineering and Applied Sciences
Harvard University
Boston, MA 02134, USA

I. Choi
Soft Robotics Research Center
Seoul National University
Seoul 08826, South Korea

M. Park, B. Jeong, Y.-L. Park
Department of Mechanical Engineering
Institute of Advanced Machines and Design
Institute of Engineering Research
Soft Robotics Research Center
Seoul National University
Seoul 08826, South Korea
E-mail: ylpark@snu.ac.kr

J. Moon, P. Pathak, J. Ahn
Department of Physical Education
Institute of Sport Science
Soft Robotics Research Center
Seoul National University
Seoul 08826, South Korea

The ORCID identification number(s) for the author(s) of this article can be found under https://doi.org/10.1002/admt.202101543.

DOI: 10.1002/admt.202101543

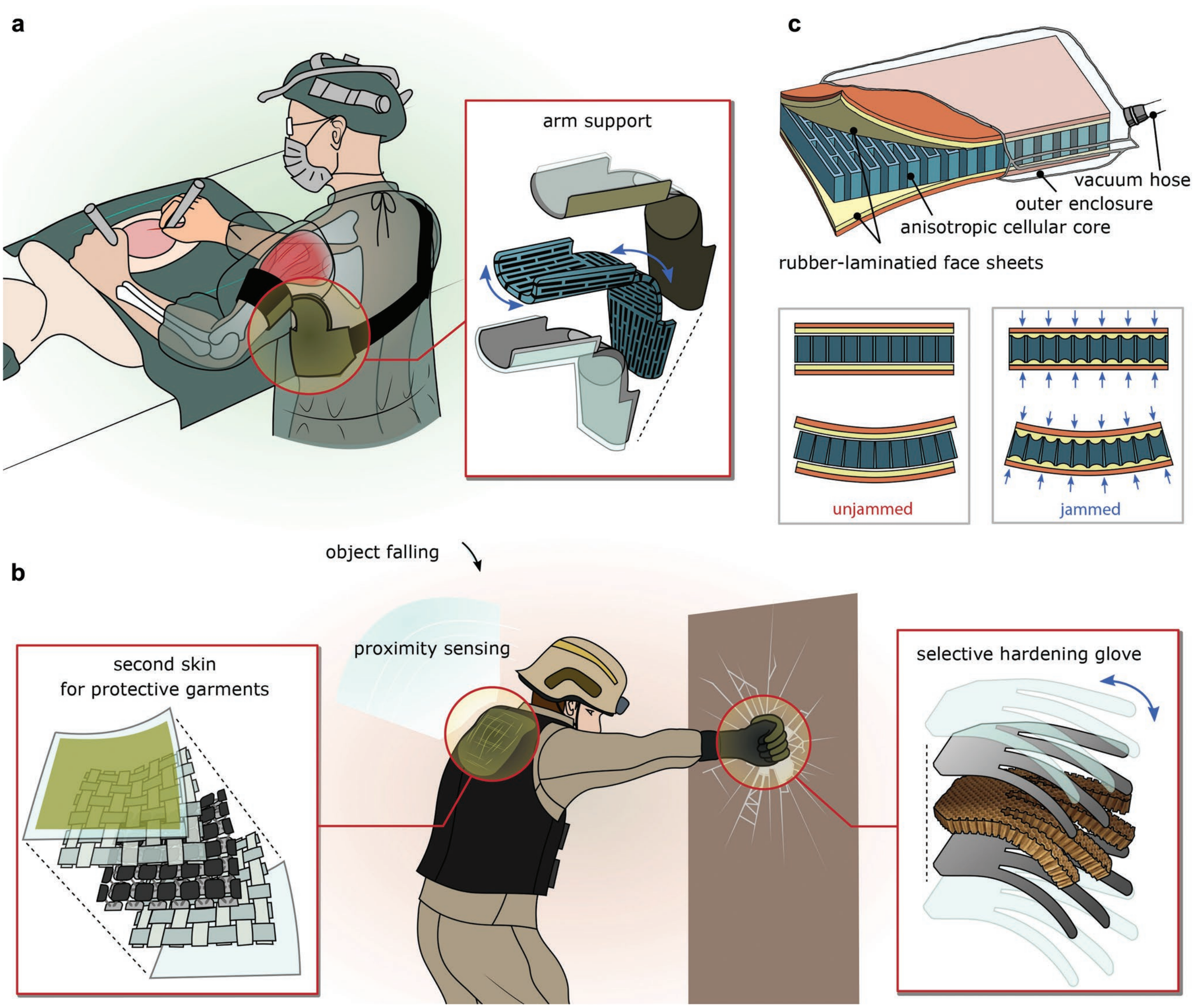

Figure 1. Two applications of selective stiffening garments with the sandwich jamming structure. a) Medical professionals, such as surgeons and dentists, are required to maintain a raised arm position while performing dexterous motions, which puts an added tension, particularly on the muscles around the shoulder girdle. An arm support to eliminate the muscle force required for weight-bearing can reduce the static-dynamic tension on the shoulder muscles. b) While the rescue workers are required to move swiftly for their missions in extreme environments, they also should be protected from unexpected collisions, and sometimes destroy obstacles to escape. A selective stiffening garment providing hard surfaces on top of skin can not only protect the wearers but also help them create a large impact force during a collision. c) The proposed sandwich jamming structure is composed of an anisotropic core and two rubber-laminated face sheets inside an outer enclosure.

be highly compliant allowing a large range of motion when deactivated. Although previously proposed jamming structures[36–37] meet part of these requirements, it is highly challenging to satisfy all while maintaining a compact form factor as a garment. The garment will be too bulky and heavy with particle jamming to provide sufficient strength due to the low force-to-weight ratio. Although layer jamming[31] provides increased stiffness, its limited degrees of freedom (DOFs) when unjammed may restrict motions, causing discomfort to wearers. This limitation has been overcome by the multi-DOF layer jamming design,[37] but additional efforts are necessary to achieve a smaller device weight and a higher bending stiffness.

To achieve high bending stiffness (or strength-to-weight ratio) when jammed but a high compliance when unjammed, we particularly focus on cellular composites,[43,44] easily found in nature.[45] They are also often employed in engineering structures, including building panels and aircraft.[43] While such industrial sandwich structures are constructed by permanent bonding of the cores to the face sheets, recent studies have shown that composite structures could be stiffened by external stimuli, such as electroadhesion[14] and vacuum-based jamming[46,47] Vacuum is an effective means of jamming sandwich structures for high structural bending stiffness. However, there has been little consideration on designs of cores and face sheets that can deform in various shapes to easily conform to different body areas when the structure is unjammed. In addition, it is necessary to provide a method of increasing the bonding force between the core and the face sheets when the structure is jammed to make the vacuum-based jamming even more effective.

In this paper, we propose a sandwich jamming structure composed of an anisotropic cellular core and rubber-laminated face sheets (Figure 1c). The lightweight anisotropic core provides a low bending modulus allowing for high structural compliance when the structure is unjammed but can be highly stiff with jamming. Compared to particle and layer jamming structures, the proposed structure provides a significantly increased performance in terms of the stiffness/strength-to-weight ratio as well as the stiffness change ratio between the unjammed and the jammed conditions (Note S1, Supporting Information). Moreover, the friction between the core and the rubber on the face sheet even further increases the bending strength. Along with the analysis and characterization, we demonstrate three SSG examples using the proposed cellular composite. The first garment, a wearable arm support, significantly reduces the muscle activation levels while not degrading the wearer's physical dexterity. In the next example, an active protector made of the SSG can quickly stiffen itself by detecting a dangerous object approaching to the wearer before collision. Lastly, we demonstrate a selective-hardening glove that can deliver a high-impact force to external objects.

2. Results

2.1. Anisotropic Cellular Core

Figure 2a shows the sandwich jamming structure with a lightweight core patterned by staggered rectangular cells. The cell geometry elongated in y-axis provides anisotropic properties for the core. The proposed core exhibits three main properties that make the jamming structure flexible in the unjammed state and rigid in the jammed state. First, the low structural modulus in x-axis $\boldsymbol{E_{xx}}$ makes the bending stiffness of the core structure considerably low, allowing for compliance similar to that of a flexure hinge, when unjammed. Second, the high modulus in z-axis $\boldsymbol{E_{zz}}$ prevents the core structure from being deformed in z-axis, maintaining the distance between the two face sheets, when jammed. Finally, the high shear modulus in the x–z plane $\boldsymbol{G_{xz}}$ minimizes shear deformation when the core and the face sheets are jammed together. The high $\boldsymbol{E_{zz}}$ and $\boldsymbol{G_{xz}}$ consequently increase the bending stiffness of the entire structure.[44]

These properties have a benefit compared to other types of structures with isotropic core materials, such as foam. Soft foam is flexible in an unjammed state but its low $\boldsymbol{E_{zz}}$ is not suitable for maintaining the gap between face sheets when a vacuum pressure is applied. The structure is also easily deformable with a shear stress due to the low $\boldsymbol{G_{xz}}$, resulting in degraded bending stiffness. Conversely, rigid foam is too stiff to allow flexibility even in an unjammed state. The sandwich jamming structure with the proposed anisotropic cellular core meets the three design requirements of lightweight, high flexibility when unjammed, and high stiffness/strength when jammed.

We first analyzed the structure with an analytical model based on the Euler–Bernoulli beam theory (Note S2, Supporting Information) and finite element analysis (FEA) (Note S3, Supporting Information). We then validated the analytical model and the FEA result through three-point bending experiments, as presented in Figure 2c. In the jammed state, the stiffnesses obtained from the model, the FEA, and the experiments were

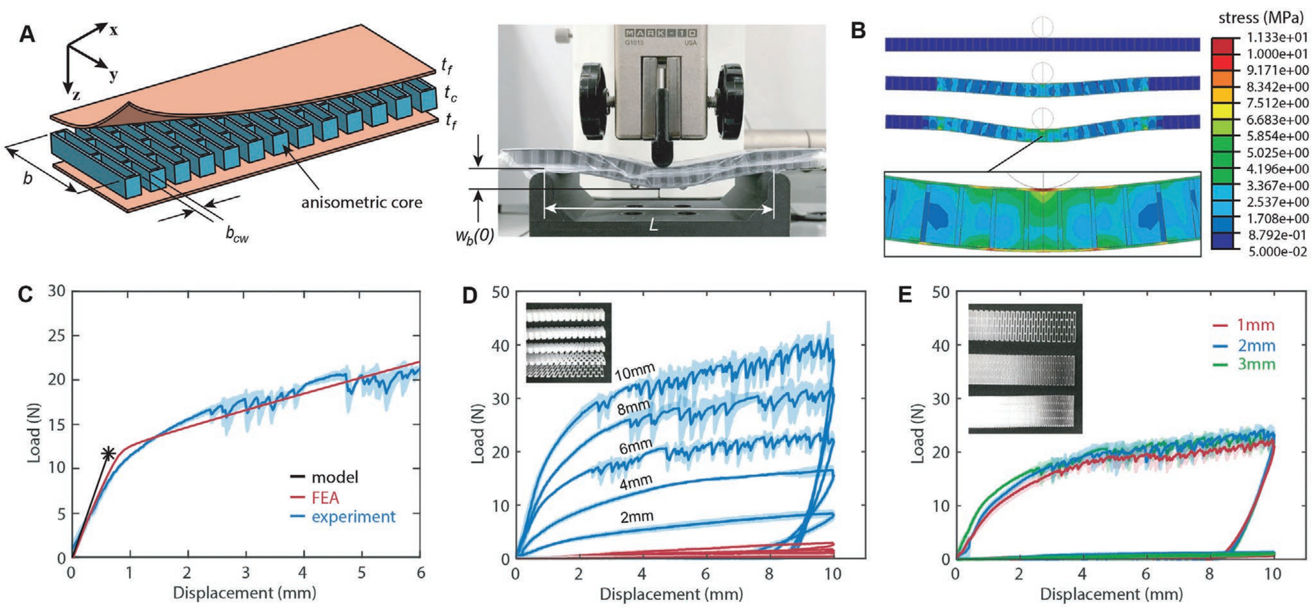

Figure 2. The effects of the anisotropic core in a sandwich jamming structure. a) Sandwich jamming structure with an anisotropic core and two face sheets. The properties of the structure were analyzed through a three-point bending test. b) Stress contour plots indicate that the stress level in the face sheets is much larger than that in the core structure. c) A comparison of the analytical model, FEA, and experimental results. d) Stiffness and yield force increased with respect to the core thickness. e) Bending stiffness did not change significantly with respect to the cellular width of the core structure.

18.6, 14.9, and 13.3 N mm^{-1}, respectively, and the yield forces were 11.7, 10.4, and 9.6 N, respectively. The differences may be due to the estimation errors in the material properties, the friction coefficients, and simplicity of our model.

The sandwich jamming structure showed an elastoplastic behavior when jammed. The entire structure acted like a solid material in the elastic region, meaning the load–displacement relation can be derived based on the Euler–Bernoulli beam theory[46] as

$$F = \frac{48}{L^3} D w_b(0) \tag{1}$$

where F is the applied load, L is the support span, D is the bending stiffness, and $w_b(0)$ is the displacement at the center of the structure.

Assuming that the Young's modulus of the face sheet E_f is much larger than that of the core E_c, and the thickness of the core t_c is much larger than that of the face sheet t_f, the approximated D is then expressed as

$$D \cong \frac{b E_f t_f t_c^2}{2} \tag{2}$$

where b is the structure width.[46] From Equations (1) and (2), the slope of the load–displacement curve in the elastic region is linearly proportional to D governed by t_c, which places the two face sheets off the neutral plane. Therefore, a high bending stiffness can be achieved by increasing the core thickness t_c (Figure 2d). The effective bending stiffness, when unjammed, can be derived by simply summing the stiffnesses of the internal components (e.g., core and face sheets) without considering their interactions.

The internal components are firmly attached to each other by friction in the elastic region. However, they slip if the in-plane shear force between the core and the face sheet exceeds the maximum static friction force, causing plastic deformation,[31,46] decreasing the bending stiffness, as observed in both FEA and experiments (Figure 2c).

The yield force F_{yield}, the transition point between the elastic and the plastic regions, can be derived as

$$F_{yield} = 2\mu_s P\, b t_c \tag{3}$$

where μ_s is the friction coefficient between the core and the face sheet, and $\boldsymbol{P}$ is the input vacuum pressure.[46] The experimental results show that the yield force is proportional to the core thickness and the vacuum pressure when the other parameters are fixed (Figure 2d and Figure S1c, Supporting Information).

Figure 2e shows the experimental results when the cellular width b_{cw} varied with a vacuum pressure of 75 kPa. Although the bending stiffness of the cellular core slightly increased when b_{cw} increased due to the effective Young's modulus, the difference was not significant. The yield forces of the three conditions are also similar. Therefore, the resisting force between the core and the face sheet can be regarded as Coulomb friction; the decrease in the contact area between the core and the face sheet was counterbalanced by the increase in the contact pressure. The results suggest that the increase in width makes the structure light and cost-efficient by reducing the density if the effective modulus of the core is small enough and no defect is on the face sheet.[43,49]

2.2. Face Sheets with Rubber Lamination

To maximize the yield strength, we can optimize design parameters, such as the friction coefficient between the internal components, the input vacuum pressure, and the core thickness. However, changing the design parameters may raise several issues: a material with high friction (e.g., rubber) has relatively low tensile and shear moduli, leading to decrease in the structural stiffness; the maximum pressure difference between the inside and the outside of the enclosure is limited to 1 atm; and increase in the core thickness increases the form factor.

To address these issues, we used a composite for the face sheet, a rubber-laminated polycarbonate sheet (**Figure 3**a). The thin rubber layer laminated on one side of the face sheet provides large friction against the core while maintaining the high modulus of the original material (i.e., polycarbonate) for resisting compression and tension. From the force-displacement plots (Figure 3b), we obtained the stiffnesses of the proposed structure using the model, the FEA, and the experiments: 15.5, 13.4, and 15.5 N mm^{-1}, respectively, and the yield forces: 31.3, 37.8, and 32.9 N, respectively (Figure 3b). The measured stiffness and the yield force increased by 17% and 243%, respectively, compared to the structure with bare face sheets (Figure 2c) although the rubber layer slightly increased the weight and the thickness.

Furthermore, the compressive force induced by jamming deforms the rubber layer and forces it to conform to the core (Figure 3c and Movie S1, Supporting Information). The geometric deformation of rubber changes the contact angle between the core and the rubber, increasing the maximum static friction by the wedge effect (or the capstan effect).[50,51] Under a normal pressure of 75 kPa, the friction coefficient between the rubber and the proposed cellular core was 5.6% higher than that between the rubber and a plain surface (Note S4, Supporting Information). In the plastic region, continuous rubber deformation occurs during sliding, increasing the friction by energy dissipation due to the hysteresis.[52,53] Otherwise, the rubber surface remains flat when unjammed so that the friction can be minimized.

We also observed that a high frequency vibration caused by stick-slip motions was substantially reduced in the plastic region (Figure 3d). This is promising, since vibrations often make robotic systems unstable during control, and it is challenging to actively eliminate them by control. We hypothesize that the reduction resulted from localized and unsynchronized stick-slip motions at the contact surface between the cells of the core and the rubber sheet.[54]

The addition of rubber also enables tuning of the mechanical properties. Figure 3e shows the characteristics of the rubber laminated face sheet with different moduli. The slope in the elastic region varied according to the modulus of the rubber layer. Considering both bending and shear deformation

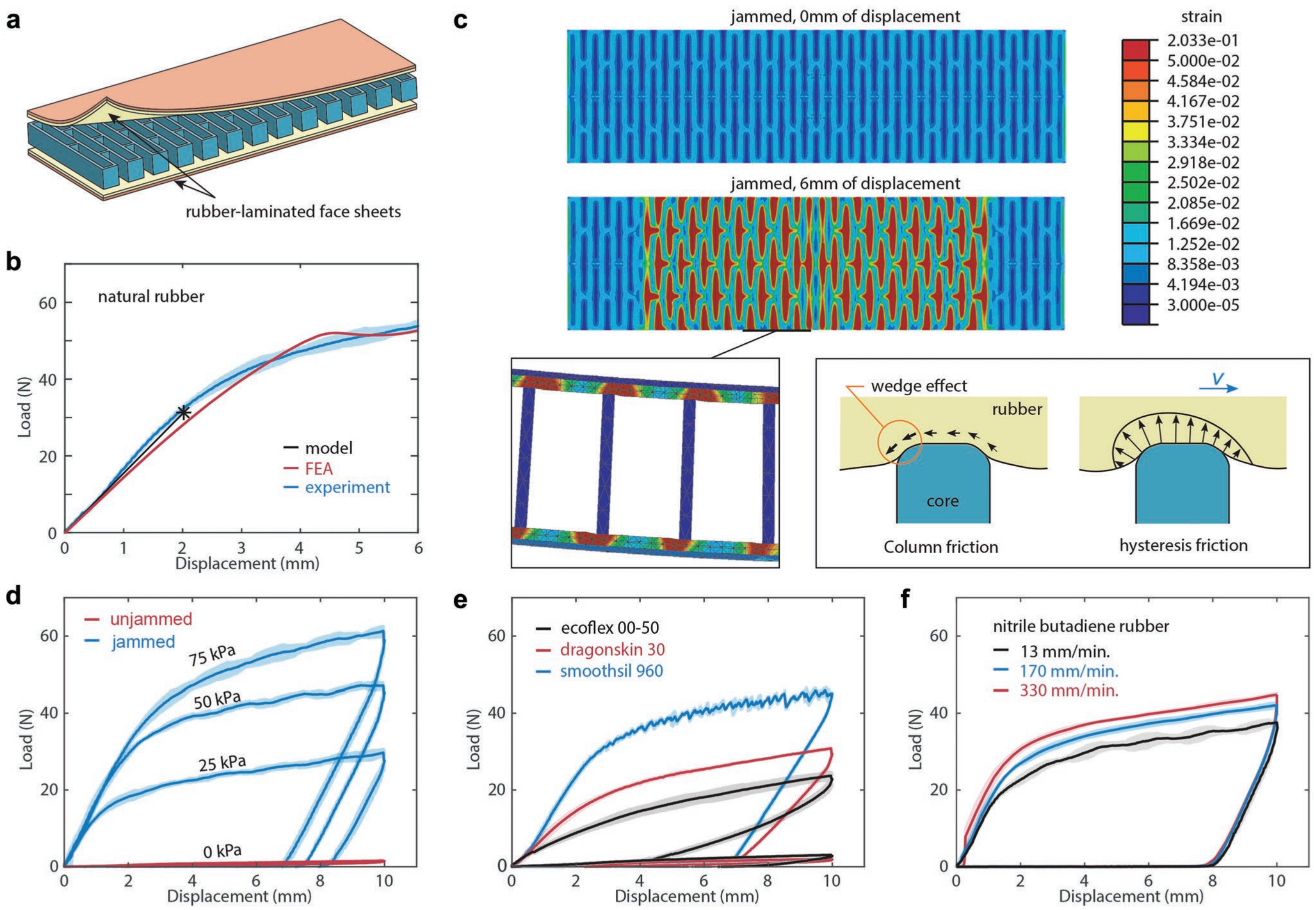

Figure 3. The effects of rubber-laminated face sheets. a) Sandwich jamming structure with rubber-laminated face sheets. b) A comparison between model, FEA, and experimental results in three-point bending tests. c) Strain contour plots indicate the soft rubber layer deforms with respect to the shape of the cellular core. This deformation of rubber can increase friction between the core and face sheets with a wedge effect. The change of rubber deformation can also increase friction with a hysteretic effect. d) Three-point bending test results with respect to the level of vacuum pressure. Natural rubber was laminated on the face sheets. e) Different performances for rubber materials with different Young's moduli. f) Jamming structure has viscoelastic bending strength with the lamination of nitrile butadiene rubber.

of rubber, the load-displacement relation of the sandwich structure is derived as

$$F = \left(\frac{L}{4S} + \frac{L^3}{48D} \right)^{-1} w(0) \tag{4}$$

$$D \cong 2bE_f t_f \left(\frac{t_c}{2} + t_r \right)^2 \tag{5}$$

$$S \cong b \frac{G_{xz,r}}{t_r} (t_c + t_f) \left(\frac{t_c}{2} + t_r \right) \tag{6}$$

where D, S, and G_r are the pure bending stiffness of the structure, the shear stiffness of the structure due to the shear deformation of the rubber sheet, and the shear modulus of the rubber (Note S2, Supporting Information), respectively. Since the modulus of the rubber affects S more dominantly than D, the different slopes in Figure 3e can be explained by the shear deformation of the rubber (Note S5, Supporting Information).

Another interesting feature of rubber lamination is viscoelasticity, shown with the sandwich structure with a laminated nitrile-butadiene rubber sheet (NBR) (Figure 3f). Rubber materials show various viscoelastic behaviors during sliding or deforming.[55,56] We tested different types of rubber materials, including natural rubber, NBR, and silicone elastomers, and NBR showed a velocity-dependent performance that was not clearly observed in the other materials. This velocity-dependent bending stiffness is useful for protection garments. When an impact is applied, the instantaneous bending stiffness is expected to be larger than that under a nonimpulsive load. The increased resisting force at a high speed is hysteretic, so the jamming structure can dissipate the impact energy more effectively.

2.3. Core and Face Sheet Designs

Figure 4 and Movie S2 (Supporting Information) shows several designs of anisotropic cores and face sheets. Human joints have a single or multiple DOFs based on the musculoskeletal

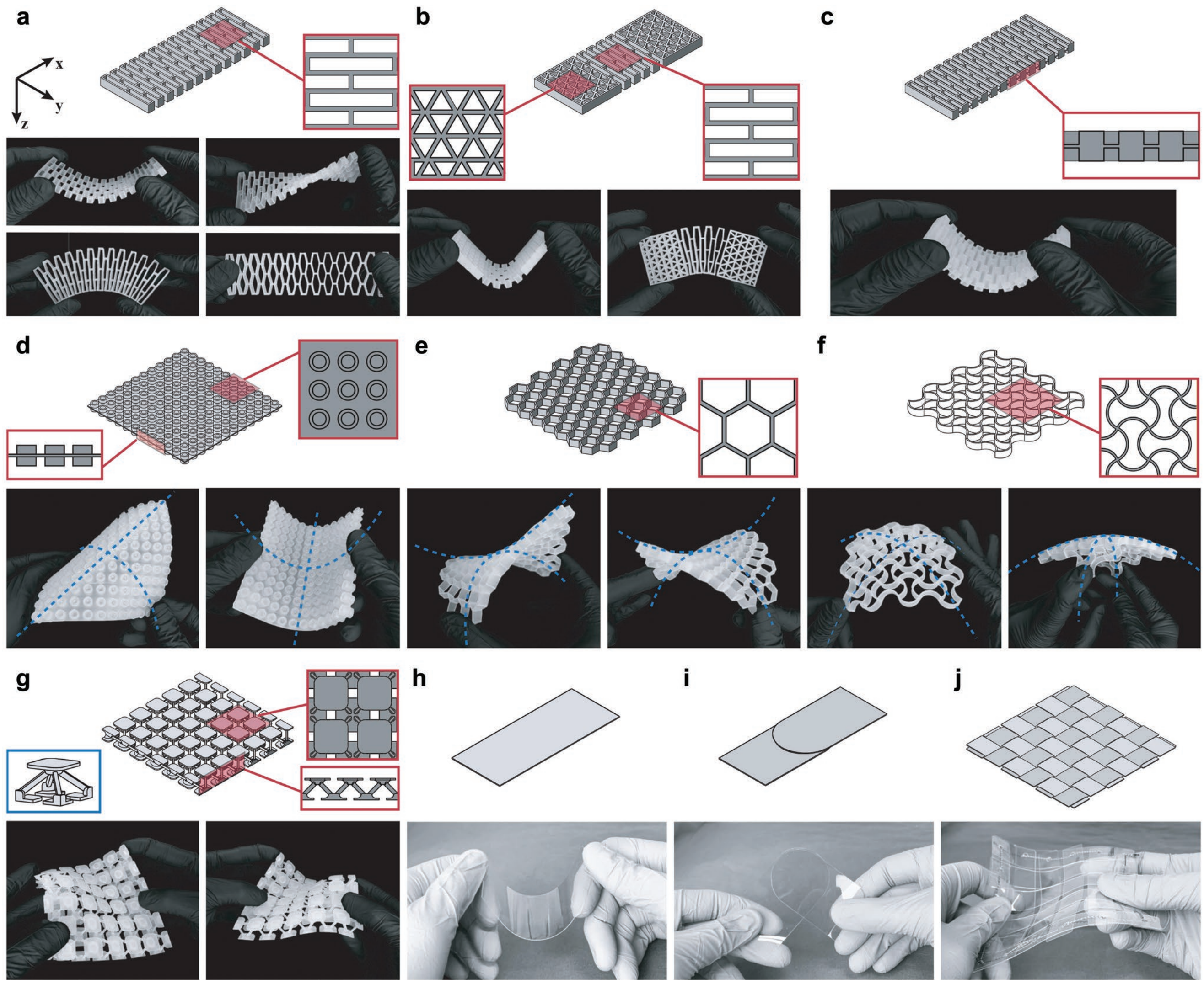

Figure 4. Anisotropic cores and face sheets with various degrees of freedom. a) Core with elongated rectangular cells. b) Core combined with elongated rectangular cells and triangular cells. c) Core with elongated rectangular cells with a thin layer in the neutral plane. d) Core with independent tubular column cells with a thin layer in the neutral plane. The Gaussian curvature is zero under the loading condition where the two ends are clamped and a single bending moment is applied about an in-plane axis. e) Core with hexagonal honeycomb cells. The Gaussian curvature is negative when deforms. f) Core composed of auxetic cells with rounded edges. The gaussian curvature is positive when deforms. g) Core with pyramidal truss structures. Each pyramidal truss has extended rectangular plates on the top and bottom surfaces. h) Single-layered face sheet. i) Double-layered face sheet. j) Face sheet woven with long thin films.

structure, and the overall shape around the joint varies. To be part of a garment, the proposed jamming composites should guarantee enough DOFs with low stiffnesses for local deformation of the target body part so that it allows for agile and dynamic motions of the wearer. This characteristic is as important as the stiffening performance when jammed.

A staggered rectangular cell pattern (Figure 4a) provides the structure with flexibility in four DOFs: bending about y- and z-axes, twisting about x-axis, and extension/compression in x-axis. When combined with a pattern of tessellating triangles that is rigid in all directions, the structure becomes partially flexible only in the middle area of the elongated rectangles (Figure 4b). This demonstrates that we can design a single core structure with different mechanical properties depending on the regions of a garment. The structure in Figure 4c is the same as that in Figure 4a except for the additional thin layer in its neutral plane. The thin layer allows a single-DOF bending motion for the structure about y-axis, while preventing other motions. These differences in DOFs of the structures are mainly determined by the anisotropic properties, having a different stiffness in each direction (Note S6 and Figure S4, Supporting Information)

Several core designs capable of more complex deformations are also demonstrated. A structure with a circular cell pattern with a thin layer in the neutral plane makes a single curvature with bending about a single axis in any direction (Figure 4d). Structures with hexagonal (Figure 4e) and auxetic (Figure 4f) cell patterns, on the other hand, make double curvatures even though they are bent about a single axis only. When the hexagonal cell structure is bent about an arbitrary axis on the plane, the structure is passively reversed about the perpendicular axis other diagonal direction. The structure becomes a hyperbolic paraboloid shape with three-point bending, meaning that the Gaussian curvature of the structure is negative (Figure S5a, Supporting Information). The auxetic cell structure with rounded edges has positive Gaussian curvature, creating a dome-shaped surface when deformed. Although these two structures form 3D shapes with double-curvature bending, each cell cannot make completely free-form deformation since the deformation of a cell affects deformations of the adjacent cells.

The core pattern can be more complex with multilayers, such as pyramidal trusses (Figure 4g). The nodes in each structural unit are flexible individually when unjammed, allowing free-form deformations, but the lightweight pyramidal structure can effectively endure compression and shear forces when jammed. Each cell's top and bottom plates are enlarged to increase the contact areas with the face sheets. The different anisotropic behaviors of the structures (Figures 4d–g) were also analyzed (Note S6, Supporting Information) with the FEA results (Figure S5, Supporting Information).

Since the jamming composite is a combination of a core and face sheets, the overall mechanical behavior varies depending on the face sheet design as well. A single layer face sheet (Figure 4h) has a low moment of inertia in thickness resulting in a low stiffness with bending about y-axis. In contrast, it has a high moment of inertia in width resulting in a high stiffness with bending about z-axis. Thus, a jamming structure with this face sheet design would be restricted for bending about z-axis although the motion is allowed for the core designs (Figures 4a,b).

The face sheet design with a combination of two layers overlapped in the middle area (Figure 4i) allows additional motions, such as bending about z-axis and extension/compression in x-axis, like a multi-DOF layer jamming structure.[37] This double-layered face sheet can be used with the cores in Figures 4a,b to allow the entire DOFs of the cores.

Since the face sheet designs in Figures 4h,i only provide single-curvature deformation, the motions of core designs with double-curvature deformations (Figure 4e,f) or free-form deformation (Figure 4g) would be restricted when they are combined together. For this reason, we propose woven face sheets (Figure 4j), similar to the structure of the jamSheet,[28] capable of adapting to various surface deformation by allowing a small movement between woven strips.

When designing new functional garments, designers can choose different combinations of the cores and the face sheets to pre-program the target properties and DOFs. For example, the pyramidal core with the woven face sheets can be applied to most areas of the human body considering its capability of free-form deformation. However, it may increase the fabrication cost and the complexity in modelling, compared to other core and face sheet designs. Some parts of the garment do not require free-from deformations if the body parts have a limited DOFs. In addition, a high bending stiffness may be more important than the DOFs in some applications. In this case, partially deformable cores would provide a better performance at a lower cost.

2.4. Application 1: Arm Support for Posture Assistance and Gravity Compensation

We demonstrate an arm support that can selectively stiffen itself to support the weight of the arms. The arm support was designed to be compact, lightweight, easy to wear, and effective in anchoring the structure to the body for distributing the load. **Figure 5**a shows the core and the face sheet designs. The sandwich jamming structure in this device is a combination of the designs in Figure 4a,i. The core employs the staggered rectangular cells and is divided into three sections. The two side sections are fixed to the upper arm and the torso, and the middle section is located under the armpit. The y-axes of the two side sections are parallel to the coronal plane of the body to easily conform to the cylindrical shapes the arm and the torso. However, the x-axis of the middle section is parallel to the coronal plane to allow multi-DOF shoulder motions, including both abduction–adduction and horizontal abduction–adduction, when unjammed (Figure 5b). When the device is jammed, the middle section is stiffened and supports the arm's weight (Figure 5c and Movie S3, Supporting Information). The device was placed under the shoulder and mounted to the body with elastic straps. When jammed, the structure effectively transmits its stiffness to the wearer's body using the large contact area. The overall weight and thickness are 290 g and 10 mm, respectively.

We hypothesize that this arm support can help operators perform manipulation tasks that require motions of raising the arms and holding the positions until they finish the tasks. In such tasks, the operator consumes a significant amount of physical and mental energy only for maintaining the fixed posture (Figure 5d). We recruited 11 participants and asked them to perform a manipulation task that require dexterity (Movie S3, Supporting Information). The process of the task consists of three main steps: picking up a grooved peg from a bin, moving it to a different area, and aligning and inserting it into a grooved hole of a pegboard. Total 25 pegs were used to complete the task. The participants performed two trials of this task for 10 min with two experimental conditions: without the support (OFF) and with the support (ON). The completion time (CT), the transverse plane of the end-effector area (EEAREA), the range of motion of each joint (ROM), and the normalized integrated electromyography ($IEMG_{NORM}$) were recorded during the tests. To analyze the muscle activities, seven electromyography (EMG) sensors were attached on the shoulder and arm muscles of the dominant arm: front deltoid (FRONT_DELT), middle deltoid (MID_DELT), rear deltoid (REAR_DELT), biceps brachii (BICEPS), triceps brachii (TRICEPS), flexor carpi radialis (FLEX_CARPI), and extensor carpi radialis brevis (EXT_CARPI).

A paired t-test revealed that the mean $IEMG_{NORM}$ values for the shoulder and the upper arm muscles were significantly lower with ON than with OFF; *FRONT_DELT*: t (10) = 3.573, $p = 0.005$; *MID_DELT*: t (10) = 3.969, $p = 0.003$; *REAR_DELT*: t (10) = 2.234, $p = 0.049$; *BICEPS*: t (10) = 2.610, $p = 0.026$; *TRICEPS*: t (10) = 2.605, $p = 0.026$ (Figure 5e). However, for the forearm muscles, there was no significant difference between the ON and OFF; *FLEX_CARPI*: t (10) = 0.215, $p = 0.834$; *EXT_CARPI*: t (10) = 0.000, $p = 1.000$. Figure 5f,g,h shows the results on CT,

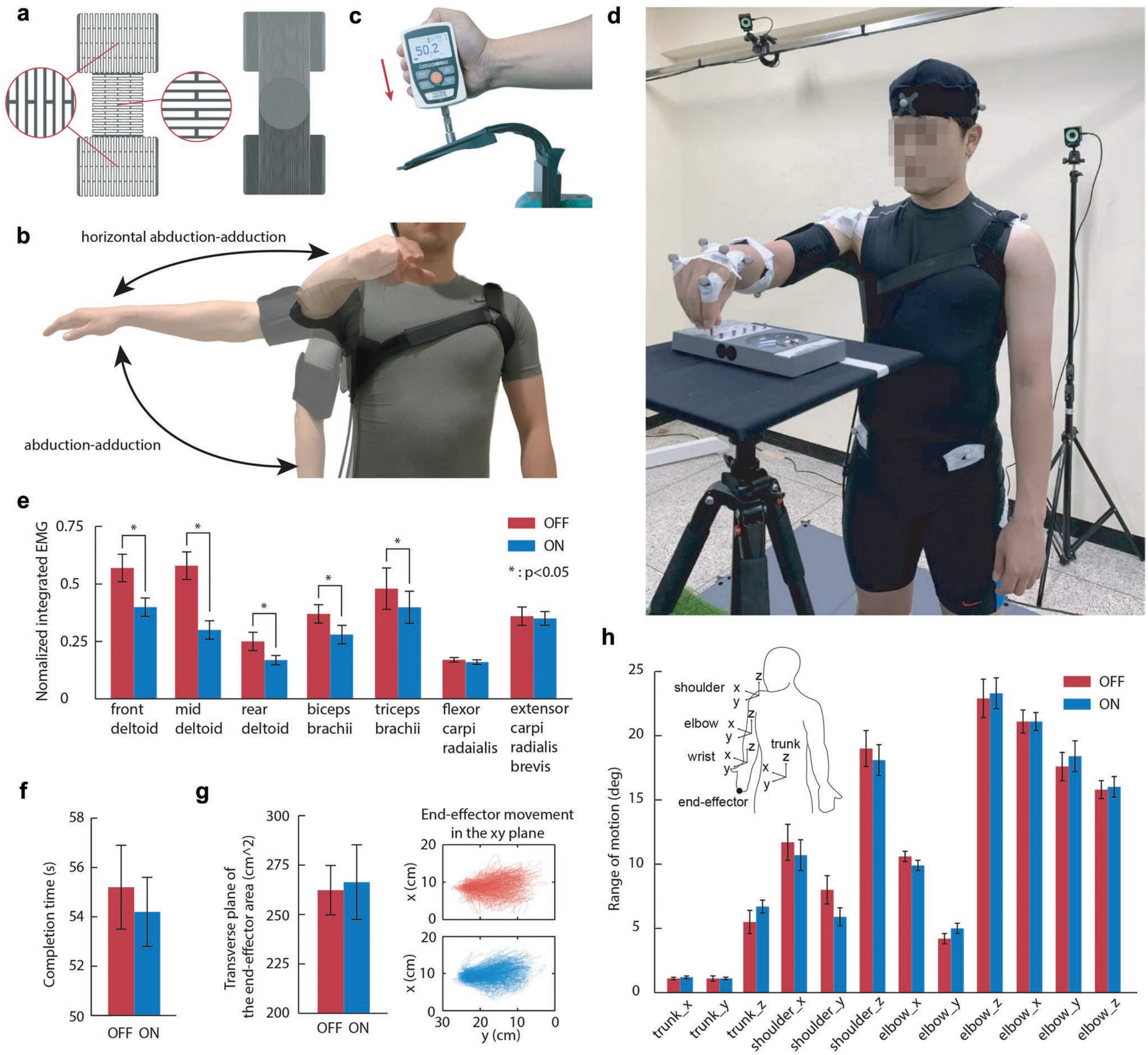

Figure 5. An arm support using the sandwich jamming structure. a) Core and face sheet designs of the arm support. b) Arm support allowing abduction–adduction and horizontal abduction–adduction motions. c) While the structure has a thin form factor, it provides sufficient stiffness and resisting force to support the arm weight. d) We conducted a precision manipulation task using a grooved peg board while requiring the wearer to maintain the arm-lifting posture with the proposed arm support. e) Reduced normalized integrated EMG values indicate that the device significantly reduced the overall muscle activity. f) Arm support did not affect the completion time for the task. g) End-effector area during the task did not change with the device. h) Range of motion of each joint did not significantly change with the device. The error bars indicate the standard deviations.

EEAREA, and ROM, respectively. There was no statistically significant difference in the mean CT, EEAREA, or the 3D ROMs of all the joints for the 11 participants between ON and OFF.

The results show that the jamming support had an effect of physical assistance, resulting in decrease in the activation levels of the shoulder and the upper arm muscles, without increasing that of the forearm muscles. In addition, CT and EEAREA results indicate that the lower activation levels of the upper arm and the shoulder muscles did not degrade the manual dexterity. No significant difference in 3D ROMs was observed between ON and OFF (Figure 5h). In summary, the proposed arm support reduced the static-dynamic muscle tension of the shoulder and the upper arm without having negative effects on the output motor performance.

2.5. Application 2: Second Skin for Protective Garments

Figure 6a shows an active protection system called "Second Skin" using the proposed sandwich jamming structure. The overall structure is flexible so that it can easily deform and fit the wearer's body parts tightly regardless of their motions

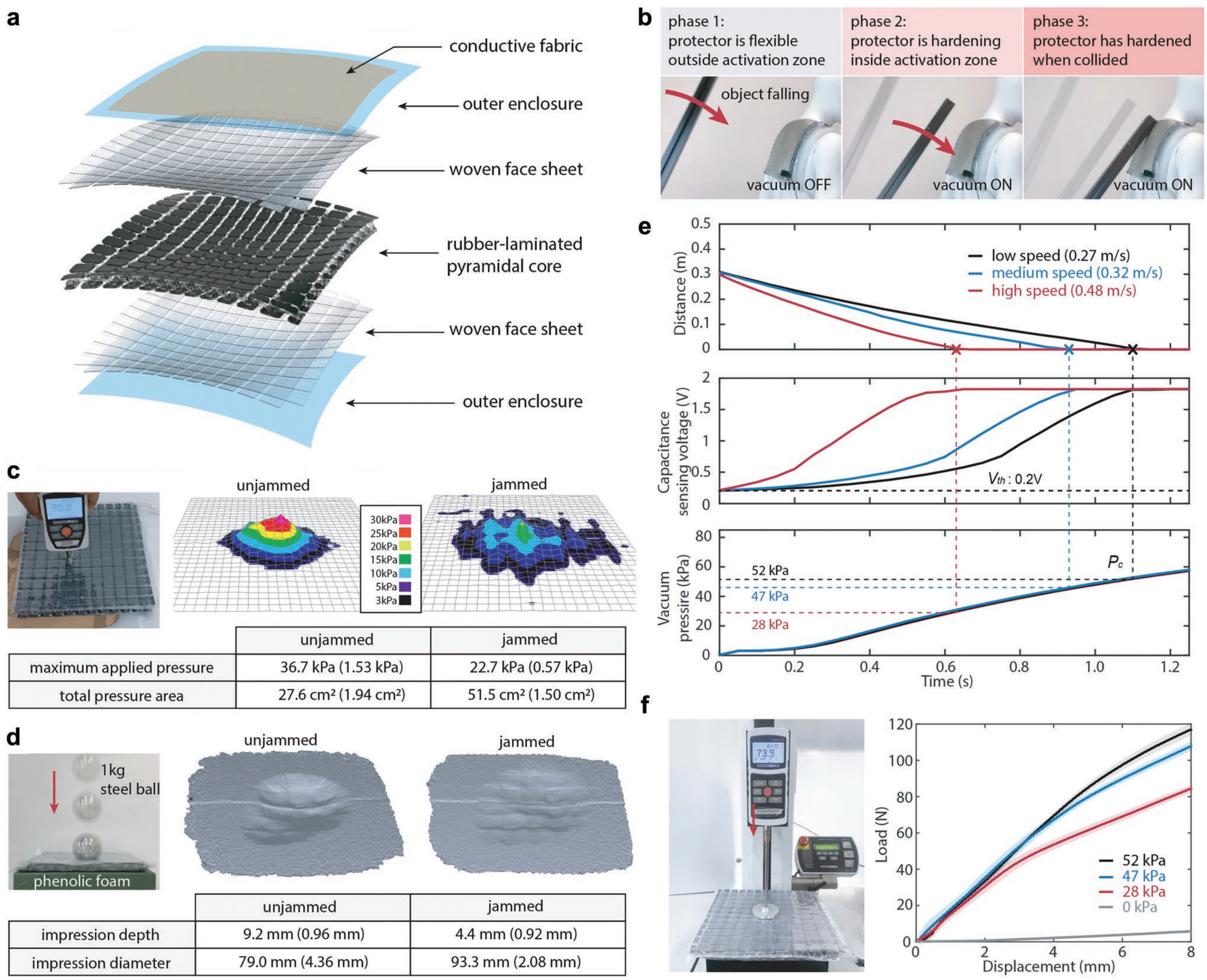

	unjammed	jammed
maximum applied pressure	36.7 kPa (1.53 kPa)	22.7 kPa (0.57 kPa)
total pressure area	27.6 cm² (1.94 cm²)	51.5 cm² (1.50 cm²)

	unjammed	jammed
impression depth	9.2 mm (0.96 mm)	4.4 mm (0.92 mm)
impression diameter	79.0 mm (4.36 mm)	93.3 mm (2.08 mm)

Figure 6. An active protector system using the sandwich jamming structure. a) Second skin composed of a rubber-laminated pyramidal core structure and woven face sheets for free-form deformation with a conductive fabric sheet and an outer enclosure. The thickness of the device is 14 mm, a form factor to be embedded in a bunker gear. b) The flexible structure deforms freely with respect to the movement and shape of the body. In case of collision with an external object, it creates hard surfaces to distribute and dissipate the impact. c) When the sandwich structure is vacuumed, it effectively distributes a 50 N static load of a 12.7 mm diameter tip. The numbers inside the parentheses indicate the standard deviations. d) When a 1 kg steel ball (diameter: 63.5 mm) falls on the structure, the vacuumed structure prevents deformation effectively. e) Demonstration of the active protector with three different approaching speeds. By reading the capacitance change of the conductive fabric sheet, the system detects the distance of the object and vacuum the structure in advance to protect the wearer. f) Protecting strengths at the vacuum pressures in e). Higher yield force was achieved with higher vacuum pressure.

or shapes. A large contact area between the structure and the wearer's body can be thus maintained even though the structure is actively hardened, facilitating distribution of a local impact caused by an unexpected collision to a larger area of the wearer's body.

The Second Skin is composed of a core layer made of rubber-laminated pyramidal elements (Figure 4g) and two woven face sheets (Figure 4h), allowing for large deformation in all directions (Figure 6b). A conductive fabric sheet was laminated on the enclosure of the jamming structure to detect external objects by capacitive proximity sensing. The form factor (overall thickness: 14 mm) is thin enough to be placed inside a regular protection garment.

Figure 6c and Movie S4 (Supporting Information) present the pressure distribution performance of the Second Skin in a static load condition. A static load of 50 N was applied using a flat, circular tip (diameter: 12.7 mm). A silicone pad (thickness: 10 mm, modulus: 69 kPa) was placed beneath the jamming structure to simulate the soft tissue of a human body. When the structure was jammed with a vacuum pressure of 75 kPa, the maximum pressure decreased by 38% by jamming while the total pressure area increased by 87%, compared to the structure with the unjammed condition.

Figure 6d and Movie S4 (Supporting Information) show the performance on a local impact. The Second Skin was placed on a phenolic foam block, which is soft and brittle that is easily

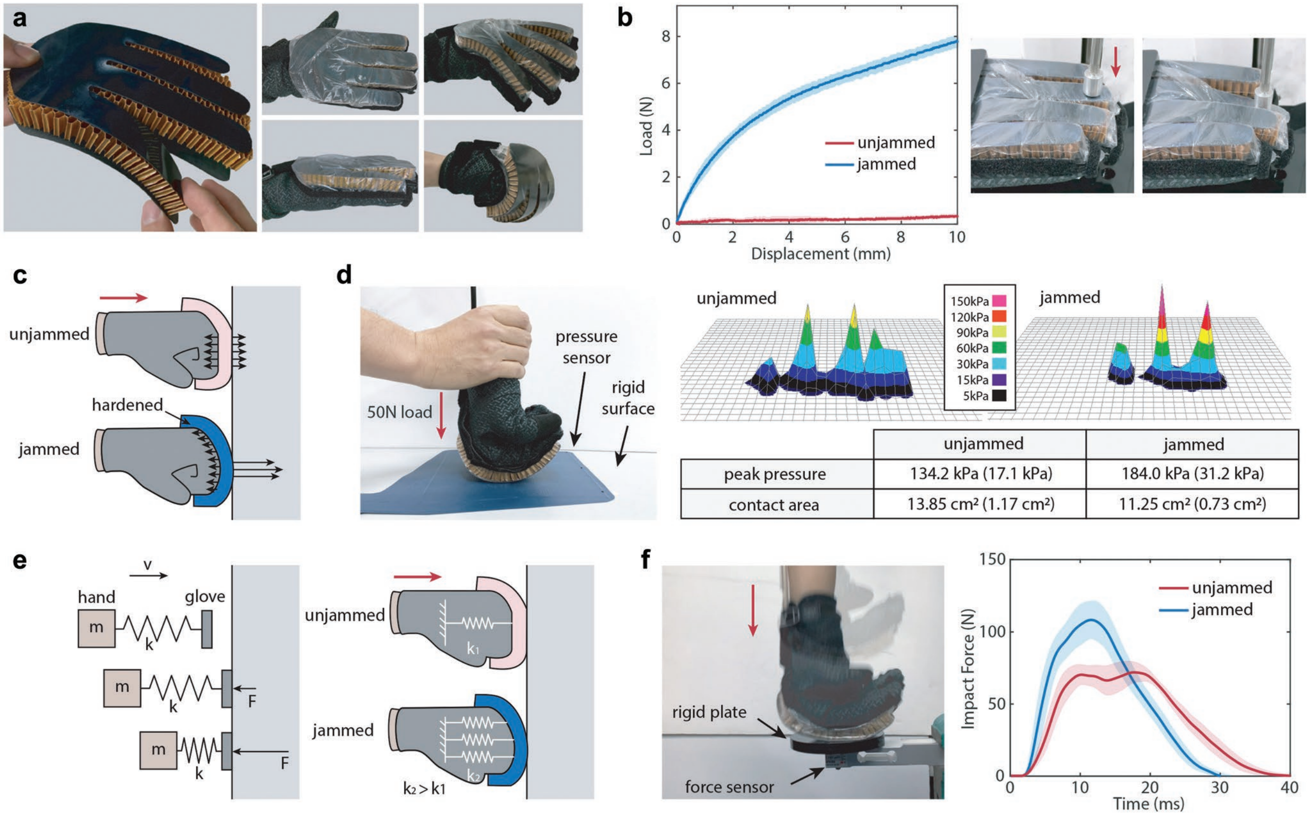

Figure 7. A selective hardening glove. a) We fabricated a sandwich jamming structure in the shape of four fingers and the back of a hand and attached to a commercial glove. When unjammed, the glove is flexible and guarantees dexterous hand movements of the wearer. When jammed, the glove hardens. b) Glove with a large stiffness difference between the unjammed and jammed conditions. c) Jammed glove not only distributes the pressure the hand receives as the protector demonstrated in Figure 6 but also increases the impact pressure applied to the local surface of an external object. d) When the glove is pressed with a 50 N load on a pressure pad, the peak pressure was increased by 37% in the jammed condition. The numbers inside the parentheses indicate the standard deviations. e) Jammed glove increases the overall stiffness of the hand during a collision due to the large hard contact area. With the increased overall stiffness, the impact force can be larger due to the reduced time constant in a collision. f) Free fall experiment measuring the amount of increased impact force. By hardening the sandwich jamming structure, the maximum force increased up to 50%.

dented by a mild impact. A 1 kg steel ball (diameter: 63.5 mm) was dropped on the device from a height of 0.5 m. When the device was unjammed, the impact created a clearly visible impression on the foam. When the device was jammed however, the depth of the impression significantly decreased while the diameter increased. The hardened surface effectively distributed the high local impact to a large area, confirming the effect of protection by reducing the peak pressure of the impact.

Figure 6e and Movie S4 (Supporting Information) demonstrate the mechanism of anticipatory collision detection and protection. The protector quickly stiffens its structure by detecting the capacitance change of the conductive fabric as the unexpected object approaches. The protector activates the vacuum valve to stiffen its structure as soon as the object reaches within 0.3 m. It corresponds to the threshold of 0.2 V, measured from a capacitance-to-voltage converter module. When an object approached at three different speeds of 0.27, 0.32, and 0.48 m s^{-1} and collided, the vacuum pressure inside the active protector reached 52, 47, and 28 kPa, respectively. Figure 6f shows the strengths of the protector at different pressure levels, and the yield forces were 61.1, 58.2, and 37.7 N, respectively.

2.6. Application 3: Selective Hardening Glove for Impact Delivery

A hard shell made of the jamming structure can be used to increase the peak impact pressure applied to an object, useful for a functional glove for destroying an object without a tool in emergency (**Figure 7**a and Movie S5, Supporting Information). While the glove allows almost free movement of the hand with dexterity due to the anisotropic flexible core when unjammed, jamming can make it hard if necessary. The result shows that the glove has large differences in stiffness and strength between the unjammed and the jammed states (Figure 7b). When unjammed, each finger can move independently with a low stiffness allowing for dexterity.

The peak impact pressure can be increased by stress concentration (Figure 7c). While the glove with high rigidity concentrates the force to a small area of the object, the reaction force from the object can be distributed to a relatively large area of the hand, similar to the result in Figure 6. A pressure pad was compressed by the prototype until the compression force reached 50 N (Figure 7d). The peak pressure was increased by 37% while the contact area was reduced by 19% by jamming.

In addition, the time constant of force delivery is reduced as the instantaneous effective stiffness increases with jamming (Figure 7e), resulting in the increase in the overall impact force with the same amount of linear momentum. We covered a soft mock-up hand with the glove and dropped it on a rigid plate from a height of 0.25 m (Figure 7f and Movie S5, Supporting Information). The impact force curves show that the jammed glove increased the average peak force by 50% compared to the unjammed one.

3. Conclusion

To realize tunable functional garments, we propose jamming-based cellular composites having high stiffness/strength-to-weight ratios and sufficient DOFs. Compared to existing jamming methods,[46,47] we achieved enhanced performances by introducing a composite face sheet structure. The rubber-laminated face sheets provide a high yield strength based on the high friction of rubber while maintaining the high stiffness due to the high modulus of the face sheet. Furthermore, multi-DOFs were realized with various anisotropic core and face sheet designs. With these improvements, our design achieved all three requirements for the SSG: lightweight, stiffness for resisting human-scale force when activated, and compliance when deactivated.

Through the experiments, theoretical modeling, and FEA, we investigated what design parameters and physical properties affect the performance. It allowed us to preprogram the mechanical properties, such as bending stiffness, yield strength, viscoelasticity, and the number of DOFs, by adjusting the geometric designs and employing multimaterial structures. This approach provides options of a wide variety of mechanical characteristics without making a substantial control effort from the viewpoint of the embodied intelligence.[57] Further investigations in modeling[58] and experimental characterization will be useful since the anisotropic structures made of different materials may include complicated interactions between the internal components. For example, the double-layered face sheet structure can be examined for the interactions between the stacked face sheets and the core. The effective friction of the woven face sheets can be analyzed, considering the changes in friction caused by the irregular and rough surface.

Three practical SSG designs showed the efficacy of the jamming-based cellular composites with a high bending stiffness/strength. Different combinations of cellular core geometry and face sheet design were selected, to accommodate the required motions of the target body parts. The jamming structure was first developed as an arm support between the upper arm and the torso. The prototype was experimentally evaluated with human subjects for a continuous planar task (dexterity test using a grooved pegboard) while a previous study had tested the performance of a static weight-bearing task with a single joint.[46] The result confirmed that the arm support significantly reduced the stress on the shoulder muscles, neither affecting the activities of other surrounding muscles nor decreasing the manual dexterity. The device allowed the wearer to work for an extended period without excessive fatigue on the shoulder. The results provided various metrics in a high-level task, reflecting more realistic working conditions. The other two applications focused on the interactions of the jamming structure to both the wearer and external objects. While the jamming structures provided sufficient DOFs before being activated, it became a hard outer shell for effectively protecting the wearer from collision and delivering high impacts to external objects. However, to be more practical further research may be necessary to detect objects with different materials from a long distance with quick activation. Device performance could be improved through early activation triggered by a proximity sensor, and a shorter response time could be achieved using a high-flow vacuum pump.

The performances of jamming-based cellular composites can be further improved with recent fabrication techniques, including metamaterials,[59] origami structure,[60] structural optimization,[61] and multimaterial 3D printing,[62] which will enable designers to fabricate precise anisotropic structures and integrate more functionalities in a compact form factor. While we focused on assisting the muscle force of the wearer under a semi-isometric condition, considering its elastoplastic behavior,[64] the jamming structure can also assist muscle activities during eccentric and concentric contractions by storing, recycling, and dissipating energy. In addition, SSGs can be combined with soft actuators, such as tendon-driven systems[10] and fluidic artificial muscles[65–67] for active assistance. We envision multifunctional and energy-efficient wearable robots enabled by the sandwich jamming approach in the future.

4. Experimental Section

Procedure of Three-Point Bending Tests: The jamming structures were characterized by the three-point bending test under a constant vacuum pressure with several steps. First, the jamming structures were placed on the fixture attached to a motorized test stand (ESM303, Mark-10) with a force gauge (M5-100, Mark-10). A vacuum pressure sensor (PSE541, SMC Korea) and a vacuum pressure regulator (ITV0091, SMC Korea) were connected to each air inlet of the jamming structure. A vacuum pump (DAA-V507-GD, GAST) produced a vacuum pressure, and the air pressure adjusted by the vacuum pressure regulator was kept constant at the desired value. Next, the test stand was lowered at a constant speed of 13 mm min^{-1}, and the displacement and the applied load were simultaneously measured. The test stand stopped and returned at the same travel speed when it reached the travel distance to 10 mm, which is enough to cover both the elastic and the plastic regions of the structure. This cycle was carried out with four different vacuum pressure levels (0, 25, 50, and 75 kPa) for different types of jamming structures. The bending tests were also conducted with three different speeds (13, 170, 330 mm min^{-1}) for the sandwich jamming structures with rubber-laminated face sheets to investigate the viscoelastic behavior. Each experimental condition was repeated three times, and the mean and the standard deviation of the load–displacement curves were calculated and plotted.

The pressure regulator and the pressure sensor were controlled and monitored by a data acquisition board (USB-6211, National Instrument), and the motorized test stand and the force gauge were controlled and monitored by a laptop. A custom-built software (Labview2015, National Instrument) was used to control all the devices and to synchronize the data measurements.

Manipulation Dexterity Test with Arm Support (Application 1): 11 healthy young adults (8 male and 3 female subjects; age: 28$\pm$3.10 years; height: 172.82$\pm$6.91 cm; weight: 66.09$\pm$11.36 kg) were recruited to participate in the study. Each participant was asked to perform the manipulative dexterity test using a grooved pegboard (Model 32025, Lafayette

Instrument).[68] The pegboard was placed on a table that was adjusted to the participant's sternum height. The participant was then asked to pick up pegs (diameter: 3 mm, length: 28 mm) from the storage area and insert them into the holes (diameter: 4 mm) in the placement area semi-continually. There were 25 pegs in total and the subject were asked to move and place only one peg at a time. As soon as the participant finished the task, the peg board was replaced with a new set so that the participant could continue the same task without stopping. The participant performed two trials of the same task continuously for 10 min, and each trial had two experimental conditions: without the arm support (OFF) and with the arm support with the jamming mechanism activated (ON). Thirty minutes of resting was provided between the trials to minimize the effect of fatigue. The sequence of the experimental conditions was randomized for each subject. The participant had three to five practice trials before the actual trials for data collection to mitigate the learning effect. During the two experimental trials, the movements of the upper body was captured using the coordinates of the 16 retro-reflective markers placed on the anatomical landmarks of the upper body. The coordinates of the retro-reflective markers were captured using 13 infrared cameras (Optitrack Prime 13, NaturalPoint Inc.). They were used to create a four-segmental model for the hand, the forearm, the upper arm, and the trunk to analyze the joint kinematics of the upper body. Muscle activation levels were also measured using surface EMG sensors for seven upper body muscles of the dominant arm; FRONT DELT, MID DELT, REAR DELT, BICEPS, TRICEPS, FLEX CARPI, and EXT CARPI. Further details for the methods and the results can be found in Note S8 (Supporting Information). The study protocol was approved by the Institutional Review Board (IRB) of Seoul National University (IRB No. 2006/002-027).

Experimental Setup for Active Wearable Protector (Application 2): The jamming structure of the active wearable protector was operated by a vacuum pump (DAA-V507-GD, GAST) through a 3-way solenoid valve (VK332V-6G-M5, SMC Korea). A vacuum pressure sensor (PSE541, SMC Korea) was connected to measure the input pressure.

In the first experiment (Figure 6c), a 10 mm thick soft silicone (Ecoflex 0030, Smooth-On) sheet was prepared to simulate the skin of the wearer's body, and the jamming structure was placed on it. A sensing pad for measuring pressure distribution (Elastisens ES-1024-160-5, Novel), composed of 32 × 32 sensors covering the sensing area of 160 × 160 mm, was installed between the jamming structure and the silicone pad. For both the jammed and the unjammed conditions, the top of the structure was locally compressed by a force gauge (M3-20, Mark-10) with a circular indenter (diameter: 12.7 mm). The pressure distribution signals were collected by a dedicated analyzer (pliance xf32, Novel) at a sampling frequency of 19 Hz. The data were transferred to a computer and processed using dedicated software (pliance x32, Novel). The test was repeated three times.

In the second experiment (Figure 6d), the jamming structure was placed on a spongy phenolic foam block (Floral Foam-Economy, Oasis) that is highly soft and brittle. A steel ball (diameter: 63.5 mm, weight: 1.0 kg) free-fell on the jamming structure from 0.5 m height during both the unjammed and the jammed states, making an impression on the foam. The shapes of the deformed foams were scanned by a 3D scanner (EinScan Pro 2X, EinScan), and the impression area and the maximum depth were measured. The test was repeated three times.

In the third experiment (Figure 6e), autonomous activation of the jamming structure was demonstrated using capacitive proximity sensing. The jamming structure was placed on the back of the mannequin, and a conductive fabric was attached to one side of the jamming structure facing outside. In this study, an extruded aluminum bar (dimension: 40 × 40 × 1000 mm, weight: 1.7 kg) hit the jamming structure at three different approaching speeds (0.27, 0.32, and 0.48 m s^{-1}). Distance between the bar and the jamming structure was analyzed using a commercial video analysis software package (ProAnalyst, Xcitex). The capacitance of the conductive fabric was measured by a capacitance-to-voltage converter module (BBCAV444, Analog Microelectronics) through shielded cables. The voltage output was measured using a data acquisition (DAQ) board (USB-6211, National Instrument). A simple control algorithm was developed to activate the jamming structure when the measured capacitance was above the preset threshold for detecting the approach of an object. The vacuum pressure inside the jamming structure was simultaneously measured by a pressure sensor (PSE541, SMC Korea) installed in the air inlet.

A separate experiment was performed to evaluate the performance of the jamming structure's stiffness/strength at difference vacuum pressures (0, 28, 47, and 52 kPa). The prototype was placed on a fixture attached to a motorized test stand with a force gauge. The fixture was designed to support the boundary of the prototype with a size of 180 × 180 mm. A flat circular tip with a diameter of 50 mm was attached to the force gauge to press the center of the prototype. The test stand was lowered at a constant speed of 13 mm/min, and the displacement and the applied load were simultaneously measured. The test was repeated three times.

Experimental Setup for Impact Test of Selective Hardening Glove (Application 3): In the first experiment (Figure 7b), the prototype was placed on a fixture attached to a motorized test stand (ESM303, Mark-10) with a force gauge (M5-100, Mark-10). The fixture was designed so that the force gauge's tip presses the middle finger of the prototype while the palm is fixed. The air inlet was connected to a vacuum pump (DAA-V507-GD, GAST) through a vacuum regulator (ITV0091, SMC Korea) to operate the jamming structure attached to the glove. For both the unjammed (0 kPa) and the jammed (75 kPa) conditions, the test stand was lowered at a constant speed of 13 mm min^{-1}, and the displacement and the applied load were simultaneously measured. The test was repeated three times.

In the second experiment (Figure 7d), the prototype was installed on a hand mock-up in fist, made of silicone. With both the jammed and the unjammed conditions, the top of the sensing pad for measuring pressure distribution (Elastisens ES-1024-160-5, Novel) was compressed by the prototype until the compression force reached 50 N. The test was repeated five times.

In the third experiment (Figure 7f), the prototype worn on the hand mock-up free-fell on a rigid plate from the height of 0.25 m with both the unjammed and the jammed states. The impact force on a rigid plate was measured by a load cell (CBCL-50L, CAS) installed beneath the plate. The force signal was transferred to a processing computer through a load cell amplifier (LCT-PRO, CAS) and a 16-bit analog-to-digital converter DAQ module (NI USB-6211, National Instruments). The sampling frequency was set to 10 kHz, enough to capture the dynamic response during the impact. The test was repeated 10 times, and the mean and the standard deviation of the peak force were calculated and plotted.

Statistical Analysis of the Human-Subject Study with Arm support: A paired t-test was used to evaluate the significant difference in CT, EEAREA, ROM, and IEMGNORM between OFF and ON conditions for the 11 participants. The level of significance was set at $p < 0.05$.

Details on the theoretical modeling, the finite element analysis, the fabrication process, and the testing methods can be found in the Supporting Information.

Supporting Information

Supporting Information is available from the Wiley Online Library or from the author.

Acknowledgements

J.K. and I.C. contributed equally to this work. This work was supported in part by the National Research Foundation (NRF) Grants (NRF-2016R1A5A1938472 and NSF-2021R1A2C2093790) funded by the Ministry of Science and ICT (MSIT) of Korea, and in part by the Technology Innovation Program (20008912) funded By the Ministry of Trade, industry & Energy (MOTIE) of Korea. The authors thank J.J.-R. Song for technical support on graphics of the main figure.

Conflict of Interest

J. Kwon, I. Choi, M. Park, B. Jeong, and Y.-L. Park are included in a Korea patent application (KR 10-2021-0115721) that covers the design and functionality of the proposed variable stiffness mechanisms with sandwich structures, which has been submitted by the SNU R&DB Foundation. The other authors declare the they have no competing interests.

Data Availability Statement

The data that support the findings of this study are available in the supplementary material of this article.

Keywords

vacuum-based jamming, sandwich jamming, variable stiffness mechanism, wearable applications

Received: November 21, 2021
Revised: February 8, 2022
Published online: March 18, 2022

[1] S. M. Watkins, L. Dunne, *Functional Clothing Design: From Sportswear to Spacesuits*, Bloomsbury Publishing, NJ, xxxx **2015**.
[2] B. Doan, Y. H. Kwon, R. Newton, J. Shim, E. V. A. Popper, R. Rogers, L. Bolt, R. Mike, W. Kraemer, *J. Sports Sci.* **2003**, *21*, 601.
[3] J. S. Michael, S. N. Dogramaci, K. A. Steel, K. S. Graham, *Gait Posture* **2014**, *39*, 804.
[4] M. T. Gross, M. K. Bradshaw, L. C. Ventry, K. H. Weller, *J. Orthop. Sports Phys. Ther.* **1987**, *9*, 33.
[5] W. J. Choi, J. A. Hoffer, S. N. Robinovitch, *Clin. Biommech.* **2010**, *25*, 63.
[6] J. L. Pons, *Wearable Robots: Biomechatronic Exoskeletons*, John Wiley & Sons, Hoboken, NJ **2008**.
[7] C. J. Walsh, K. Endo, H. Herr, *Int. J. Hum. Rob.* **2007**, *4*, 487.
[8] D. Kim, B. B. Kang, K. B. Kim, H. Choi, J. Ha, K. J. Cho, S. Jo, *Sci. Rob.* **2019**, *4*, eaav2949.
[9] Y.-L. Park, B. Chen, N. Perez-Arancibia, D. Young, L. Stirling, R. J. Wood, E. C. Goldfield, R. Bioinspir, *BioinspirationBiomimetics* **2014**, *9*, 016007.
[10] J. Kwon, J.-H. Park, S. Ku, Y. Jeong, N.-J. Paik, Y.-L. Park, *IEEE Robot. Autom. Lett.* **2019**, *4*, 2547.
[11] C. Laschi, B. Mazzolai, M. Cianchetti, *Sci. Rob.* **2016**, *1*, eaah3690.
[12] S.-J. Kim, D.-Y. Lee, G.-P. Jung, K.-J. Cho, *Sci. Rob.* **2018**, *36*, eaar2915.
[13] J. De Vicente, D. J. Klingenberg, R. Hidalgo-Alvarez, *Soft Matter* **2011**, *7*, 3701.
[14] L. Di Lillo, D. Carnelli, A. Bergamini, S. Busato, P. Ermanni, *Smart Mater. Struct.* **2011**, *20*, 057002.
[15] A. Firouzeh, M. Salerno, J. Paik, *IEEE Trans. Rob.* **2017**, *33*, 765.
[16] S. Rich, S.-H. Jang, Y.-L. Park, C. Majidi, *Adv. Mater. Technol.* **2017**, *2*, 1700179.
[17] B. E. Schubert, D. Floreano, *RSC Adv.* **2013**, *3*, 24671.
[18] A. J. Liu, S. R. Nagel, *Nature.* **1998**, *396*, 21.
[19] M. Cates, J. Wittmer, J.-P. Bouchaud, P. Claudin, *Phys. Rev. Lett.* **1998**, *81*, 1841.
[20] U. Knaack, T. Klein, M. Bilow, *Deflatables*, Publishers, xxxx **2008**, p. 010.
[21] A. Cavallo, M. Brancadoro, S. Tongnarelli, A. Menciassi, *Soft Rob.* **2019**, *6*, 161.
[22] S. Chopra, M. T. Tolley, N. Gravish, *IEEE Rob. Autom. Lett.* **2020**, *5*, 3975.
[23] H. M. Jaeger, *Soft Matter.* **2015**, *11*, 12.
[24] T. Liu, H. Xia, D.-Y. Lee, A. Frouzeh, Y.-L. Park, K.-J. Cho, *IEEE Rob. Autom. Lett.* **2021**, *6*, 8078.
[25] M. Brancadoro, M. Manti, F. Grani, S. Tognarelli, A. Menciassi, M. Cianchetti, *Front. Rob. AI* **2019**, *6*, 12.
[26] M. Brancadoro, M. Manti, S. Tognarelli, *Soft Rob.* **2020**, *7*, 663.
[27] S. Jadhav, M. R. A. Majit, B. Shih, J. P. Schulze, M. T. Tolley, *Soft Rob.* **2021**, 9, 173.
[28] J. Ou, L. Yao, D. Tauber, J. Steimle, R. Niiyama, H. Ishii, presented at *ACM Int. Conf. Tang. Embedd. Embod. Inter. Munich*, February 16–19, **2014**.
[29] M. Ibrahimi, L. Paternò, L. Ricotti, A. Menciassi, *Soft Rob.* **2021**, *8*, 85.
[30] I. Choi, N. Corson, L. Peiros, E. W. Hawkes, S. Keller, S. Follmer, *IEEE Rob. Autom. Lett.* **2017**, *3*, 450.
[31] Y. S. Narang, J. J. Vlassak, R. D. Howe, *Adv. Funct. Mater.* **2018**, *28*, 1707136.
[32] Y. Wang, L. Li, D. Hofmann, J. E. Andrade, C. Daraio, *Nature* **2021**, *596*, 238.
[33] A. Sadeghi, A. Mondini, B. Mazzolai, *Actuators* **2019**, *8*, 47.
[34] V. Wall, R. Deimel, O. Brock, presented at *IEEE Int. Conf. Robot. Autom*, xxxx, Seattle May 25–30, **2015**.
[35] Y. Yang, Y. Zhang, Z. Kan, J. Zeng, M. Y. Wang, *Soft Rob.* **2019**, *7*, 292.
[36] S. Hauser, M. Robertson, A. Ijspeert, J. Paik, *IEEE Rob. Autom. Lett.* **2017**, *2*, 849.
[37] W. H. Choi, S. Kim, D. Lee, D. Shin, *IEEE Rob. Autom. Lett.* **2019**, *4*, 2539.
[38] D. S. Shah, E. J. Yang, M. C. Yuen, E. C. Huang, R. Kramer-Bottiglio, *Adv. Funct. Mater.* **2021**, *31*, 2006915.
[39] T. Mitsuda, S. Kuge, M. Wakabayashi, S. Kawamura, *Pres. Tele. Virt. Env.* **2002**, *11*, 569.
[40] E. Brown, N. Rodenberg, J. Amend, A. Mozeika, E. Steltz, M. R. Zakin, H. Lipson, H. M. Jaeger, *Proc. Natl. Acad. Sci. USA* **2010**, *107*, 18809.
[41] A. Jiang, T. Ranzani, G. Gerboni, L. Lekstutyte, K. Althoefer, P. Dasgupta, T. Nanayakkara, *Soft Rob.* **2014**, *1*, 192.
[42] Y.-J. Kim, S. Cheng, S. Kim, K. Iagnemma, *IEEE Trans. Rob.* **2013**, *29*, 1031.
[43] D. Zenkert, *An Introduction to Sandwich Construction*, xxxx, Oxford, Chameleon **1995**.
[44] L. J. Gibson, M. F. Ashby, *Cellular Solids: Structure and Properties*, Cambridge Univ. Press, Cambridge **1999**.
[45] L. J. Gibson, M. F. Ashby, B. A. Harley, *Cellular Materials in Nature and Medicine*, Cambridge Univ. Press, Cambridge **2010**.
[46] Y. S. Narang, B. Aktas, S. Ornellas, J. J. Vlassak, R. D. Howe, *Soft Rob.* **2020**, *7*, 724.
[47] D. C. F. Li, Z. Wang, B. Ouyang, Y. H. Liu, presented at *IEEE Int. Conf. Robot. Autom*, xxxx, Montreal, May 20–24, **2019**.
[48] F. Huijben, *Vacuumatics: 3D Formwork Systems*, Eindhoven University of Technology, Netherlands **2014**.
[49] F. C. CampbellJr., *Manufacturing Technology for Aerospace Structural Materials*, Elsevier, Amsterdam **2011**.
[50] A. J. Loeve, T. Krijger, W. Mugge, P. Breedveld, D. Dodou, J. Dankelman, *Wear* **2014**, *319*, 27.
[51] P. Gabriel, A. Thomas, J. Busfield, *Wear* **2010**, *268*, 747.
[52] A. Schallamach, *Wear* **1971**, *17*, 301.
[53] G. Heinrich, M. Klüppel, *Wear* **2008**, *265*, 1052.
[54] Y. Kligerman, M. Varenberg, *Tribol. Lett.* **2014**, *53*, 395.
[55] K. A. Grosch, *Rubber Chem. Technol.* **1964**, *37*, 386.
[56] G. A. D. Briggs, B. J. Briscoe, *Wear* **1975**, *35*, 357.
[57] R. Pfeifer, M. Lungarella, F. Iida, *Science.* **2007**, *318*, 1088.
[58] P. Szeptyński, *Compos. Struct.* **2020**, 112088.
[59] C. Coulais, E. Teomy, K. De Reus, Y. Shokef, M. Van Hecke, *Nature* **2016**, *535*, 529.

[60] A. A. Deleo, J. O'Neil, H. Yasuda, M. Salviato, J. Yang, *Compos. Sci. Technol*. **2020**, *191*, 108060.
[61] C. Schumacher, S. Marschner, M. Gross, B. Thomaszewski, *ACM Trans. Graph*. **2018**, *37*, 148.
[62] M. A. Skylar-Scott, J. Mueller, C. W. Visser, J. A. Lewis, *Nature* **2019**, *575*, 330.
[63] C. de Marco, S. Pané, B. J. Nelson, *Sci. Rob*. **2018**, *3*, 287.
[64] S. H. Collins, M. B. Wiggin, G. S. Sawicki, *Nature* **2015**, *522*, 212.
[65] J. Wirekoh, L. Valle, N. Pol, Y.-L. Park, *Soft Rob*. **2019**, *6*, 768.
[66] J. Kwon, S. J. Yoon, Y.-L. Park, *IEEE Trans. Rob*. **2020**, *36*, 743.
[67] K. Narumi, H. Sato, K. Nakahara, Y. Seong, K. Morinaga, Y. Kakehi, R. Niiyama, Y. Kawahara, *IEEE Rob. Autom. Lett*. **2020**, *5*, 3915.
[68] Y. C. Wang, S. R. Magasi, R. W. Bohannon, D. B. Reuben, H. E. McCreath, D. J. Bubela, W. Z. Rymer, *J. Hand Ther*. **2011**, *24*, 313.
[69] R. M. Wang, S. R. Zheng, Y. G. Zheng, *Polymer Matrix Composites and Technology*, Elsevier, Amsterdam **2011**.
[70] M. K. Mohamed, A. A. ElKattan, W. A. Ali, *Int. J. Eng. Tech*. **2012**, *12*, 144.
[71] S. Maegawa, F. Itoigawa, T. Nakamura, *Trib. Int*. **2015**, *92*, 335.
[72] L. Oliveira, D. Simpson, J. Nadal, *Physiol. Meas*. **1996**, *17*, 305.
[73] M. P. Furmanek, S. Solnik, D. Piscitelli, O. Rasouli, A. Falaki, M. L. Latash, *J. Motor Behav*. **2018**, *50*, 492.

